PHYSICAL REVIEW C **95**, 054606 (2017)

Global phenomenological optical model potential for ^{8}Li projectile

XinWu Su,[1] YinLu Han,[2,*] HaiYing Liang,[2] ZhenDong Wu,[2] HaiRui Guo,[3] and ChongHai Cai[4]
[1]*College of Physics and Electronic Science, Shanxi Datong University, Datong 037009, China*
[2]*Key Laboratory of Nuclear Data, China Institute of Atomic Energy, P.O. BOX (275-41), Beijing 102413, China*
[3]*Institute of Applied Physics and Computational Mathematics, Beijing 100094, China*
[4]*Department of Physics, Nankai University, Tianjin 300071, China*

(Received 29 October 2016; revised manuscript received 5 April 2017; published 8 May 2017)

A set of global phenomenological optical model potential parameters for ^{8}Li projectile is obtained by fitting the experimental data of ^{8}Li elastic-scattering angular distributions from ^{9}Be to ^{208}Pb targets with incident energies between 11.0 and 33.1 MeV. By using the global optical model potential obtained, the elastic-scattering angular distributions are calculated and compared with the available experimental data. It is shown that the ^{8}Li global potential can achieve satisfactory reproduction of the experiment.

DOI: 10.1103/PhysRevC.95.054606

I. INTRODUCTION

The optical model potential (OMP) is one of the most fundamental theoretical tools in the study of nuclear reactions. The phenomenological OMP is widely adopted in practice, because it can be easily extracted by fitting the experimental data of elastic scattering [1]. In particular, the global phenomenological OMP is specified for both a mass region and an energy region [2], so it can be used to reliably calculate reaction cross sections and elastic-scattering angular distributions in some energies and nuclide regions, where no experimental data exist.

The reactions involving short-lived radioactive nuclear beams (RNBs) are of intrinsic interest in nuclear physics and nuclear astrophysics. Due to the existence of the weakly bound neutron-halo or proton-halo in the RNB projectile, the direct transfer or breakup processes dominate in the energy region below the barrier. Recently, many experiments involving weakly bound and short-lived radioactive halo nuclei have been done and present extremely interesting features, such as ^{6}He, ^{8}B. In particular, the short-lived radioactive nucleus ^{8}Li is also an interesting subject to study within the context, which has a small separation energy of 2.0 MeV for the valence neutron in the $p_{3/2}$ state. The reaction induced by the light neutron-rich nucleus ^{8}Li is intensively studied both theoretically and experimentally due to its important role in our understanding of the nucleosynthesis [3]. It has also been found to be important to produce seed nuclei for the *r* process, e.g., in type-II supernovae [4]. Likewise, the ^{8}Li-induced reactions can have important consequences for the abundances of ^{6,7}Li and other light nuclei [5].

When we research these reactions involving the ^{8}Li nucleus incidence or emission with a range of targets, the global phenomenological OMP for ^{8}Li is very important for us to understand the reaction mechanism. Furthermore, some key reactions involving the ^{8}Li nucleus in the nuclear astrophysics are very difficult or even impossible to measure directly with current facilities. Therefore, it is necessary to construct a set of global phenomenological OMP parameters for ^{8}Li with a wide range of targets, which will further provide a theoretical guide for the reaction with respect to the weakly bound nucleus ^{8}Li scattering. Up to now, more and more intermediate-energy data on the elastic scattering of ^{8}Li projectile over wide target mass number range $9 \leqslant A \leqslant 208$ have become available.

In this paper, a global phenomenological OMP for ^{8}Li projectile is derived based on the experimental elastic-scattering angular distributions from ^{9}Be to ^{208}Pb targets with incident energies below 40 MeV. It is based on a smooth, unique functional form for the energy dependence of the potential depths and physically constrained geometry parameters. Furthermore, the elastic-scattering angular distributions are calculated and compared with the corresponding experimental data.

The paper is organized as follows: In Sec. II, we present the basic phenomenological OMP formula and the functional form of the energy and radial dependencies for the real and imaginary potentials and parameters. Section III shows the comparison of our results with experimental data. Finally, we give the conclusions in Sec. IV.

II. THE OPTICAL MODEL POTENTIAL AND PARAMETERS

A. Form of optical model potential

The phenomenological OMP is defined as the sum of the real and imaginary parts of potentials as well as the Coulomb potential

$$V(r,E) = V_R(r,E) + i[W_S(r,E) + W_V(r,E)] + V_C(r), \quad (1)$$

where V_R, W_S, and W_V are the real part, the imaginary part of surface and volume absorption potential. $V_C(r)$ is the Coulomb potential. E is the is the laboratory energy of the incident particle in MeV. The real and imaginary parts of potentials are separately composed of E-dependent well depths V_R, W_S, W_V, and energy-independent radial parts; namely, the form factor. The most widely used form factors are Woods–Saxon shape for the real and imaginary parts of potentials. The spin-orbit potential is neglected in the present analysis.

---

[*] hanyl@ciae.ac.cn

The real part of OMP is expressed as

$$V_R(r,E) = -\frac{V_R(E)}{1+\exp\left[(r-R_R)/a_R\right]}. \tag{2}$$

The imaginary part for surface absorption of OMP is

$$W_S(r,E) = -4W_S(E)\frac{\exp[(r-R_S)/a_S]}{\{1+\exp[(r-R_S)/a_S]\}^2}. \tag{3}$$

The imaginary part for volume absorption of OMP is

$$W_V(r,E) = -\frac{W_V(E)}{1+\exp\left[(r-R_V)/a_V\right]}. \tag{4}$$

The Coulomb term V_C is usually taken from the electric field of a spherical homogeneous charge density nucleus with radius R_C,

$$V_C(r) = \begin{cases} \frac{zZe^2}{2R_C}\left(3-\frac{r^2}{R_C^2}\right), & r < R_C \\ \frac{zZe^2}{r}, & r \geqslant R_C, \end{cases} \tag{5}$$

where Z and z are the charge of the target and projectile, respectively.

The energy dependence of the potential depth is expressed as the simplest polynomial form,

$$V_R(E) = V_0 + V_1E, \tag{6}$$

$$W_S(E) = W_0 + W_1E, \tag{7}$$

$$W_V(E) = U_0 + U_1E. \tag{8}$$

The radii are given by

$$R_i = r_iA^{\frac{1}{3}}, \quad i = R,S,V,C, \tag{9}$$

where r_R, r_S, r_V, and r_C are the radius parameters of the real part, the imaginary part of surface absorption, the imaginary part of volume absorption, as well as the Coulomb potential. A is the mass number of the target. The quantities a_R, a_S, and a_V are the corresponding diffuseness width. The 13 parameters V_0, V_1, W_0, W_1, U_0, U_1, r_R, r_S, r_V, r_C, a_R, a_S, and a_V can be adjusted.

B. Parametrization of optical model potential

All experimental data of elastic-scattering angular distributions for ^{8}Li projectile are collected and analyzed, which include those targets for the mass $9 \leqslant A \leqslant 208$. They are from the nuclear EXFOR database [6]. The available elastic-scattering angular distributions are just below 40 MeV. The complete experimental database of elastic-scattering angular distributions for ^{8}Li is detailed in Table I.

The experimental data of elastic-scattering angular distributions are simultaneously fit by the improved code APMN [7], which can automatically search global phenomenological OMP parameters on the basis of the improved fastest falling method [8] at incident energies below 300 MeV. It is well known that the discrete ambiguities commonly encounters in the optical model parametrization of the elastic scattering for strongly absorbed projectiles. Thus, we first give all the potential parameters reasonable boundaries of the varied region by some physical limitation before the global phenomenological OMP parameters are automatically searched. In the process of the adjustment, the best OMP parameters are simultaneously performed to minimize a quantity called χ^2, which represents the deviation of the calculated results from the experimental values and is defined as follows:

$$\chi^2 = \frac{1}{N}\sum_{i=1}^{N}\left[\frac{\sigma_i^{th}-\sigma_i^{ex}}{\Delta\sigma_i^{ex}}\right]^2, \tag{10}$$

where N is the number of data points for each angular distribution. σ_i^{th} and σ_i^{ex} are the theoretical calculations and the experimental values of differential cross sections, as well as the $\Delta\sigma$ is the experimental error of corresponding data. The uncertainty of experimental data is taken from the nuclear database EXFOR [6]. On the basis of the elastic-scattering angular distributions in the mass range $9 \leqslant A \leqslant 208$, as well as by using the improved optimization procedure, the global phenomenological OMP parameters for ^{8}Li projectile are obtained and are given in Table II.

TABLE I. The $d\sigma/d\Omega$ database for ^{8}Li elastic scattering. The E_{in} is the incident energy for different targets in the laboratory system, except for ^{208}Pb in the mass-center system. The χ^2 value is given for each angular distribution.

Target	E_{in}(MeV)	χ^2	Ref.
^{9}Be	14	2.68	[9]
	19.6	13.26	[10]
	27	11.29	[11]
^{12}C	14	0.69	[9]
	23.9	2.57	[12]
^{13}C	14	0.69	[9]
^{14}N	14	0.38	[9]
^{27}Al	14	0.21	[9]
^{51}V	18.5	1.61	[10]
	26	1.94	[13]
^{58}Ni	14	1.18	[9]
	19.6	5.93	[9]
	20.2	5.17	[13]
	22	9.51	[13]
^{197}Au	14	4.09	[9]
^{208}Pb	24.4	6.73	[14]
	27.9	3.59	[14]
	28.9	1.95	[14]
	30.6	4.63	[14]
	33.1	13.01	[14]

III. CALCULATED RESULTS AND ANALYSIS

In this section, we first analyze the global OMP for ^{8}Li projectile. Then, the elastic-scattering angular distributions are calculated by using the global phenomenological OMP obtained for ^{8}Li below 40 MeV. These results are further compared with the corresponding experimental data.

The radial *dependencies* on the real part and imaginary part of global OMP are calculated for different targets at incident energies of 20, 50, 100, 150, 200, 250, and 300 MeV. It is found that the absolute value of the real part decreases with increasing radius and incident energy. The absolute value of imaginary

TABLE II. The global phenomenological OMP parameters for ^{8}Li projectile.

Parameter	Value	Units
V_0	187.615	MeV
V_1	− 0.513	
W_0	33.417	MeV
W_1	− 0.132	
U_0	12.329	MeV
U_1	0.378	
r_R	1.232	fm
r_S	1.462	fm
r_V	1.800	fm
a_R	0.786	fm
a_S	0.920	fm
a_V	0.527	fm
r_C	1.572	fm

part increases first and then decreases with increasing incident radius. These results for ^{58}Ni are given in Fig. 1. It can be seen that the depth of the real part of the potential decreases with increasing incident energy. The contribution to imaginary part of global OMP changes from the dominant surface absorption into the volume absorption with increasing incident energy.

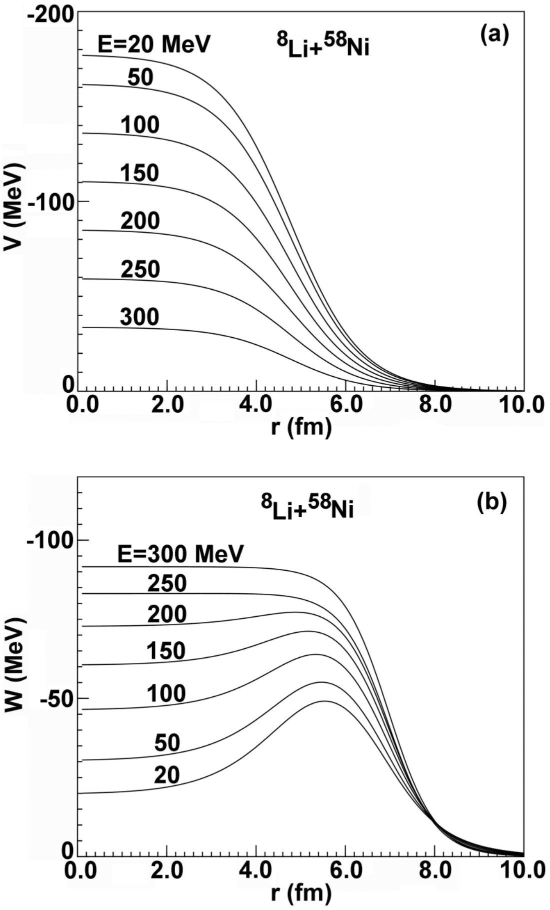

FIG. 1. The radial dependence of our global OMP at incident energies of 20, 50, 100, 150, 200, 250, and 300 MeV for ^{58}Ni: (a) real part, (b) imaginary part.

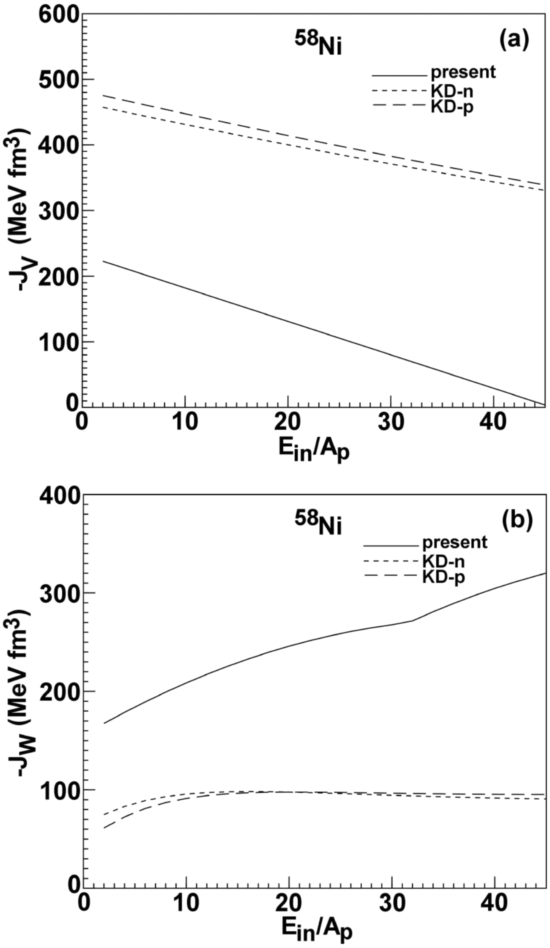

FIG. 2. Comparison between volume integrals of per nucleon for ^{58}Ni target calculated by using the ^{8}Li global OMP (solid curve) and neutron (short-dashed curve) or proton global OMP (dashed curve). The energies have been scaled to E_{in}/A_P with $A_P = 8$ for ^{8}Li and $A_P = 1$ for neutron or proton: (a) real part J_V, (b) imaginary part J_W.

Another important quantity in the study of OMP is the volume integral of potential. The volume integral per nucleon of OMP is defined as

$$J_V = \frac{1}{A_p A_T}\int V_R(E,\vec{r}\,)d\vec{r}, \tag{11}$$

$$J_W = \frac{1}{A_p A_T}\int \left[W_S(E,\vec{r}\,) + W_V(E,\vec{r}\,)\right]d\vec{r}, \tag{12}$$

where A_p and A_T are the mass numbers for projectile and target, respectively.

The ^{8}Li volume integrals per nucleon of real part and imaginary part through our global phenomenological OMP are calculated for different targets. Figure 2 shows these results for ^{58}Ni. It is observed that the volume integral per nucleon of real part J_V is linearly dependent on the incident energy and decreases with increasing incident energy. However, the total absorption volume integral per nucleon J_W is opposite. Simultaneously, the volume integrals per nucleon for ^{58}Ni are

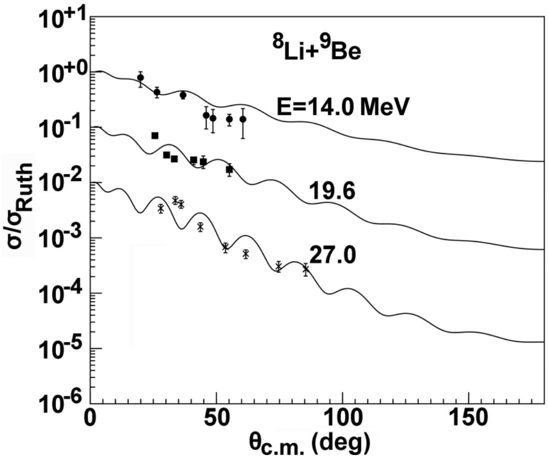

FIG. 3. Comparison between the optical model calculations (solid lines) and experimental data [9–11] of elastic-scattering angular distributions for ^{9}Be at different energies of the laboratory system. The curve and data points at the top represent true values, while the others are offset by factors of 10^{-1}, 10^{-2}, and so on.

compared between ^{8}Li global phenomenological OMP and the widely used global neutron or proton phenomenological optical model potential KD [2] in Fig. 2. For the volume integral of real part J_V, both optical potentials are linearly dependent on the incident energy of per nucleon and decrease with increasing incident energy, while the volume integrals per nucleon of imaginary part J_W have different energy dependence between them. Our optical potential rapidly increases with increasing incident energy. The reason may be that the projectile ^{8}Li is taken as a group in our global phenomenological OMP.

The elastic-scattering angular distributions are figured out by using ^{8}Li global OMP for different targets and compared with the existing experiment data. The χ^2 values of each angular distribution from the obtained global OMP parameters of ^{8}Li are also given in Table I.

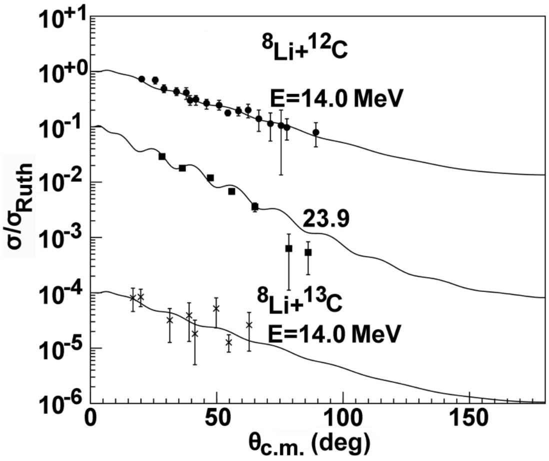

FIG. 4. Same as Fig. 3, but for ^{12,13}C [9,12], and the other data are offset by factors of 10^{-1}, 10^{-4}.

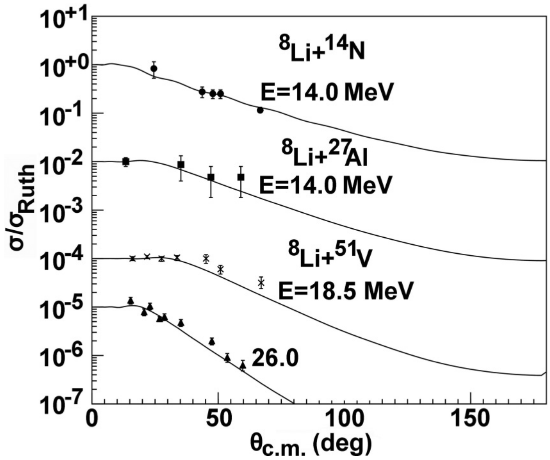

FIG. 5. Same as Fig. 3, but for ^{14}N, ^{27}Al, ^{51}V [9,10,13]; the other data are offset by factors of 10^{-2}, 10^{-4}, 10^{-5}.

Figure 3 presents the comparison with the experimental data [9–11] for ^{9}Be at different incident energies. It is seen that this potential gives a good fit for these angular distributions at different incident energies, especially for 14.0 MeV.

Figure 4 presents the comparison of the elastic-scattering angular distributions in the Rutherford ratio with the experimental data [9,12] for ^{12,13}C at 14.0 and 23.9 MeV. The close agreements between them are achieved within the experiment error.

The elastic-scattering angular distributions for ^{14}N, ^{27}Al, and ^{51}V are calculated by the global phenomenological OMP parameters. The comparisons between the calculations and experiment data [9,10,13] for them are shown in Fig. 5. From this figure, we can see that this potential reproduces well the elastic-scattering angular distributions for them.

The elastic-scattering angular distributions for ^{58}Ni are also calculated. The results compared with the experimental data [9,13] from 14.0 to 22.0 MeV are shown in Fig. 6. At all incident energies of ^{8}Li, the agreement between them is generally good. The similar results are also obtained for ^{197}Au at 14.0 MeV.

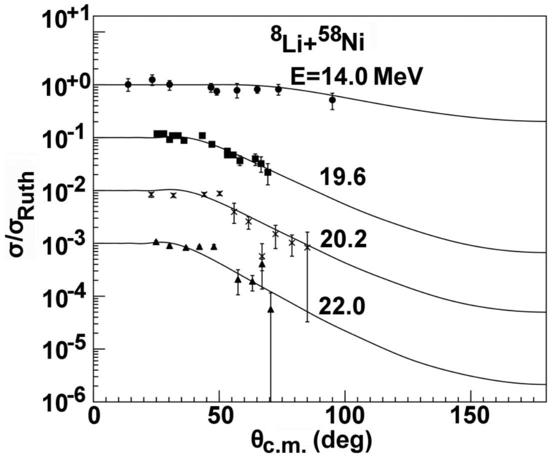

FIG. 6. Same as Fig. 3, but for ^{58}Ni [9,13].

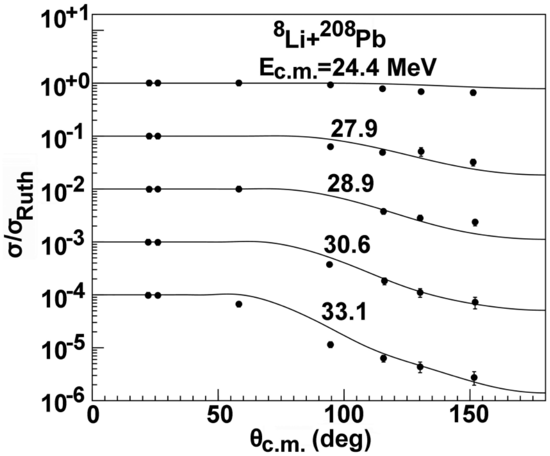

FIG. 7. Same as Fig. 3, but for ^{208}Pb at different energies of the mass-center system [14].

TABLE III. The same as Table I, but for the total reaction cross sections. σ_{th} and σ_{ex} are the theoretical results calculated using our ^{8}Li global OMP and the data extracted from the elastic-scattering angular distribution analysis by using different optical model potentials, respectively.

Target	E_{in}(MeV)	σ_{th}(mb)	σ_{ex}(mb)	Ref.
^{9}Be	19.6	1714	1332	[10]
^{12}C	14.3	1593	1169	[12]
^{51}V	18.5	1561	975	[10]
	26.0	2042	1657	[13]
^{208}Pb	24.4	66	225	[14]
	27.6	499	504	[14]
	28.89	660	624	[14]
	30.57	924	885	[14]
	33.13	1270	1219	[14]

The calculations of elastic-scattering angular distributions for ^{208}Pb are compared with the experimental data [14] from 22.4 to 33.1 MeV in the mass-center system, as shown in Fig. 7. From the figure, we can see that the results are also in *reasonable* agreement with experimental data.

Furthermore, there are *no* experimental data of total reaction cross sections below 40 MeV. But some data [10,12–14] of total reaction cross sections were extracted from the elastic-scattering angular distribution analysis using different optical model potentials for ^{9}Be, ^{12}C, ^{51}V, and ^{208}Pb. The comparisons between optical model calculations and some data of total reaction cross sections are made for them, which are given in Table III. It can be seen that our ^{8}Li OMP gives a good description in the error range for some energy points while there are some discrepancies between them. The reason is that our results are from the global optical model potential.

IV. SUMMARY AND CONCLUSIONS

We have constructed a set of physically constrained and global phenomenological OMP parameters for ^{8}Li projectile based on the available experimental data of the elastic-scattering angular distributions for some targets. We systematically analyze elastic scattering for ^{8}Li projectiles below 40 MeV by the obtained global phenomenological OMP and compare with the corresponding experimental data. Our research provides a good description for the elastic-scattering angular distributions just below 40 MeV. Thus, the obtained global OMP of ^{8}Li are reliable below 40 MeV. At higher incident energies, the reliability of global MOP need to *be verified* by new experimental data. Good agreements of OMP with experimental data show that our global phenomenological OMP will be significative to make systematic studies for nuclear model calculations and experimental analysis involving ^{8}Li scattering, especially for the breakup or transfer reactions.

ACKNOWLEDGMENTS

This work is supported by China National Natural Science Foundation under Grant No. 11405099 and No. 11575291. This work is also a part of IAEA Coordinated Research Projects (CRPs) on Recommended Input Parameter Library (RIPL) for Fission Cross Section Calculations under Contract No. 20464.

[1] P. E. Hodgson, *The Optical Model of Elastic Scattering* (Clarendon, Oxford, 1963).
[2] A. J. Koning and J. P. Delaroche, Nucl. Phys. A **713**, 231 (2003).
[3] L. V. Grigorenko, B. V. Danilin, V. D. Efros, N. B. Shulgina, and M. V. Zhukov, Phys. Rev. C **57**, R2099(R) (1998).
[4] M. Terasawa, K. Sumiyoshi, T. Kajino, G. J. Mathews, and I. Tanihata, Astrophys. J. **562**, 470 (2001).
[5] F. D. Becchetti, W. Z. Liu, D. A. Roberts *et al.*, Phys. Rev. C **40**, R1104(R) (1989).
[6] www-nds.iaea.org/exfor/exfor.htm
[7] Q. B. Shen, Nucl. Sci. Eng. (La Grange Park, IL, U. S.) **141**, 78 (2002).
[8] B. Alder, S. Fernbach, and M. Rotenberg, *Methods in Computational Physics* (Academic Press, New York, 1966).
[9] F. D. Becchetti, W. Z. Liu, K. Ashktorab *et al.*, Phys. Rev. C **48**, 308 (1993).
[10] S. Mukherjee, N. N. Deshmukh, V. Guimaraes *et al.*, Eur. Phys. J. A **45**, 23 (2010).
[11] V. Guimaraes, R. Lichtenthaler, O. Camargo *et al.*, Phys. Rev. C **75**, 054602 (2007).
[12] A. Barioni, V. Guimaraes, A. Lepine-Szily *et al.*, Phys. Rev. C **80**, 034617 (2009).
[13] A. Lepine-Szily and R. Lichtenthaler, Nucl. Phys. A **787**, 94C (2007).
[14] J. J. Kolata, V. Z. Goldberg, L. O. Lamm *et al.*, Phys. Rev. C **65**, 054616 (2002).